Journal of Applied Informatics and Computing (JAIC)
Vol.10, No.2, April 2026, pp. 1416~1425
e-ISSN: 2548-6861

From Global GPS to Local Waypoints: A UTM-Based GPS-IMU Localization Method for VTOL UAV Navigation

Ryan Satria Wijaya [1]*, Nedia Waty [2], Nur Rafia Dija [3]***
* Depaertement of Electrical Engineering Batam State Polytechnic, Batam, Indonesia
ryan@polibatam.ac.id [1], nediawaty390@gmail.com [2], dija@polibatam.ac.id [3]

Article Info

Article history:

Received 2026-01-31
Revised 2026-02-27
Accepted 2026-03-04

Keyword:

GPS,
IMU,
Localization,
UTM,
VTOL UAV.

ABSTRACT

This study presents a deterministic UTM-based GPS–IMU localization framework for short-range waypoint navigation of a Vertical Take-Off and Landing (VTOL) unmanned aerial vehicle. Unlike conventional GNSS–IMU approaches that rely on tightly coupled probabilistic fusion algorithms, the proposed method emphasizes coordinate transformation efficiency for relative waypoint consistency under open-sky conditions. GPS latitude–longitude data from a standalone u-blox M10 receiver are converted into Universal Transverse Mercator (UTM) coordinates and transformed into a local Cartesian reference frame to enable efficient distance and bearing computation. Heading information is obtained from IMU yaw measurements embedded in the Pixhawk 6C flight controller. Experimental validation was conducted in an open-sky environment using five predefined waypoint positions per trial. Performance was evaluated using Root Mean Square Error (RMSE) and sample standard deviation metrics. The system achieved distance RMSE values of 0.030 m, 0.047 m, and 0.017 m across three scenarios, while bearing RMSE remained within 4–5°, satisfying the predefined benchmark (distance RMSE < 0.1 m; bearing RMSE < 5°). These results reflect short-range relative geometric consistency rather than absolute GNSS positioning accuracy. The findings demonstrate that deterministic UTM-based coordinate transformation combined with GPS–IMU heading estimation provides stable short-range waypoint consistency without requiring additional probabilistic fusion algorithms.

I. INTRODUCTION

Unmanned aerial vehicles (UAVs) have experienced rapid growth in autonomous navigation applications, particularly in missions requiring precise waypoint tracking and position stability [1]. Among various UAV configurations, quadcopters are widely adopted due to their mechanical simplicity, vertical take-off and landing capability, and high maneuverability. The symmetric four-rotor configuration enables stable hovering and accurate motion control, making quadcopters suitable for missions that demand precise localization and directional stability. This study employs a UAV platform aligned with the specifications commonly used in the Indonesian Flying Robot Contest (KRTI), particularly in the Vertical Take-Off and Landing (VTOL) division. In this category, UAVs are required to autonomously execute waypoint-based missions in open-field environments [2]. The success of these missions strongly depends on the reliability and stability of the navigation and localization system [3]. Accurate estimation of both position and orientation is therefore essential to ensure precise waypoint tracking and consistent directional control.

Localization refers to the process of determining a vehicle's position within a defined coordinate framework. In UAV navigation, this involves transforming global position measurements into a coordinate representation suitable for local motion control. A robust localization system must provide real-time and numerically stable position estimates, as these estimates form the basis for computing distance and bearing toward predefined waypoints [4].

Satellite-based positioning systems, commonly referred to as Global Navigation Satellite Systems (GNSS), are widely

used in UAV navigation due to their broad coverage and ease of integration. In this study, a standalone GPS module is employed; therefore, the term GPS is used consistently to describe the positioning component of the proposed system, while GNSS is retained only when referring to related work in the literature. GPS measurements are susceptible to multipath effects, signal obstruction, and environmental interference [5], [6]. Moreover, GPS does not directly provide reliable orientation information required for directional control.

To complement position estimation, orientation and angular motion information are obtained from an Inertial Measurement Unit (IMU), which integrates accelerometer and gyroscope measurements. The yaw angle derived from the IMU serves as the heading reference for waypoint navigation. Although IMUs provide high update rates and independence from external signals, standalone inertial estimation is subject to cumulative drift due to integration errors. Without correction, this drift can result in significant long-term deviation [7]. Therefore, effective integration of GPS-based position data and IMU-based heading information is necessary to maintain consistent navigation performance.

In practical waypoint navigation, GPS latitude–longitude measurements are typically transformed into a planar coordinate system to simplify motion-control calculations. The Universal Transverse Mercator (UTM) projection provides a two-dimensional Cartesian representation expressed in meters, enabling direct Euclidean distance and bearing computation toward a target waypoint [8]. This transformation from global geodetic coordinates to a local Cartesian representation forms the computational foundation for efficient waypoint navigation.

Although GNSS–IMU integration has been extensively studied in UAV navigation research, most existing approaches rely on tightly coupled probabilistic sensor-fusion frameworks, such as the Extended Kalman Filter (EKF), Unscented Kalman Filter (UKF), or GNSS/INS integration schemes, to enhance robustness and absolute positioning accuracy. These methods primarily aim to minimize global state-estimation error under dynamic or GNSS-degraded conditions. However, limited attention has been given to experimentally isolating and evaluating the role of coordinate representation in short-range waypoint navigation performance.

In lightweight UAV systems operating under open-sky conditions, where GPS availability is relatively stable, the use of full probabilistic state-estimation frameworks may introduce unnecessary computational overhead and parameter-tuning complexity. Furthermore, prior studies rarely investigate whether deterministic coordinate transformation alone can provide sufficient relative distance and bearing consistency for short-range waypoint missions. Direct geodetic computation using latitude–longitude coordinates also involves nonlinear trigonometric operations that may reduce numerical efficiency in embedded real-time implementations.

Consequently, the specific contribution of coordinate transformation efficiency remains unclear, as filtering and projection representation are typically evaluated simultaneously. Therefore, a research gap exists in systematically investigating whether a UTM-based local Cartesian transformation, integrated with GPS–IMU heading estimation, can achieve stable short-range waypoint navigation without relying on complex probabilistic fusion algorithms.

To address this gap, this study formulates a measurable hypothesis: a deterministic UTM-based coordinate transformation integrated with GPS–IMU heading estimation can maintain short-range waypoint navigation consistency with a distance RMSE below 0.1 m and a bearing RMSE within 5° under open-sky conditions. Rather than benchmarking against probabilistic EKF-based fusion in terms of absolute global positioning accuracy, this study defines a practical technical benchmark focused on relative waypoint consistency and computational simplicity. The proposed framework is evaluated against this predefined short-range navigation performance threshold to determine whether complex state-estimation filtering is strictly necessary for open-field VTOL missions.

II. METHOD

This section describes the research stages undertaken to develop and evaluate the proposed localization system for the VTOL UAV platform. The methodology consists of mechanical configuration design, system architecture development, localization implementation, and experimental performance evaluation.

A. Mechanical Configuration

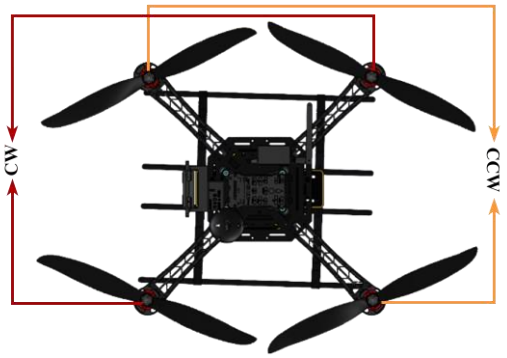

Figure 1. VTOL Propulsion Layout and Propeller Rotation Directions

A quadcopter-type VTOL UAV was employed as the experimental platform. The vehicle is equipped with four brushless motors and four propellers arranged in a symmetric frame structure. As shown in Figure 1, the propulsion system follows a crossed rotation configuration, where two propellers rotate clockwise (CW) and the other two rotate counterclockwise (CCW) [9], [10]. This opposing rotation balances motor torque and ensures stable flight dynamics,

providing a reliable platform for evaluating the proposed localization system.

Figure 2. GPS Sensors and IMU Placement

This study employs two primary sensors: a GPS module and an Inertial Measurement Unit (IMU) [11]. Their configuration and placement are illustrated in Figure 2. The GPS module is mounted on the top of the drone frame to optimize satellite signal reception, while the IMU is integrated into the Pixhawk 6C flight controller as an internal component [12]. The Pixhawk 6C incorporates an onboard IMU consisting of a 3-axis gyroscope and a 3-axis accelerometer (ICM-42688-P), along with an internal magnetometer for heading estimation. The IMU provides orientation information, particularly the yaw angle, which serves as the heading reference in the VTOL navigation system.

The positioning system utilizes a u-blox M10 GNSS receiver operating in standalone mode without RTK or differential correction. The receiver provides latitude and longitude measurements at approximately 5 Hz, with a typical horizontal accuracy of 1.5–2.0 m under open-sky conditions according to manufacturer specifications.

B. System Block Diagram

The block diagram of the system used in this study is shown in the figure below.

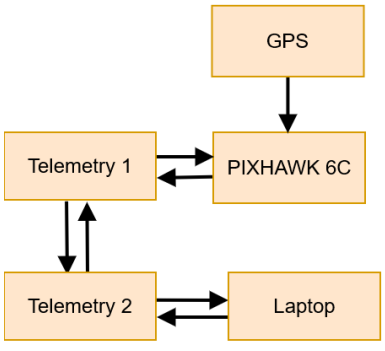

Figure 3. Localization System Block Diagram

The system architecture of the proposed localization framework is illustrated in Figure 3. The Pixhawk 6C flight controller serves as the central control and data processing unit of the VTOL UAV. The GPS module is directly connected to the Pixhawk to provide latitude and longitude measurements, which are subsequently transformed into UTM (X, Y) coordinates for position representation in meters and navigation analysis. The system incorporates two telemetry modules for wireless communication. Telemetry 1 is connected to the Pixhawk, while Telemetry 2 interfaces with a laptop. Through this bidirectional link, GNSS position data and IMU-derived orientation data, particularly yaw (heading), are transmitted in real time to the laptop for monitoring, processing, and data logging.

No custom sensor-fusion algorithm was implemented in this study. The system relies solely on the default Extended Kalman Filter (EKF) embedded within the Pixhawk firmware for attitude stabilization and basic state estimation. The internal EKF structure was neither modified nor redesigned. The primary contribution of this research lies in the deterministic UTM-based coordinate transformation and relative waypoint computation using GNSS position outputs and IMU heading data provided by the flight controller.

C. Localization

The proposed localization system applies a waypoint-based navigation method, in which predefined coordinate points serve as flight destinations for the UAV [13]. The system utilizes position data obtained from a Global Positioning System (GPS) sensor and orientation data provided by an Inertial Measurement Unit (IMU) [14]. The GPS module provides geographic position measurements in the form of latitude and longitude coordinates [15]. These geographic coordinates are subsequently transformed into the Universal Transverse Mercator (UTM) coordinate system to obtain planar Cartesian coordinates expressed in meters along the X (Easting) and Y (Northing) axes.

Since the experiments were conducted in Batam, Indonesia (approximately 1° N, 104° E), all geographic coordinates were converted using UTM Zone 48N. During experimentation, both the UAV position and the predefined waypoint were represented in the UTM coordinate system. The transformation from latitude–longitude coordinates to UTM coordinates was performed using equations 1 and 2.

Easting

$$X = k_0 N(\mathrm{A} + \alpha A^3 + \beta A^5) + 500000 \quad (1)$$

Northing

$$Y = k_0 \left(M + N \tan \emptyset \left(\frac{A^2}{2} + \ + \gamma A^4 + \delta A^6 \right) \right) \quad (2)$$

For the Easting component, X represents the position in the east–west direction within the UTM coordinate system. The parameter k_0 denotes the scale factor at the central meridian, while N represents the radius of curvature in the prime vertical at latitude $\emptyset$. The variable A corresponds to the

longitude difference between the point and the central meridian of the UTM zone. The higher-order terms αA^3 and βA^5 are included to improve projection accuracy by compensating for Earth curvature effects [16]. The constant value $+500000$ m represents the false easting applied to ensure that all Easting coordinates within a UTM zone remain positive.

For the Northing component, Y represents the position in the north–south direction in meters. The term M denotes the meridional arc length, defined as the distance from the equator to latitude $\emptyset$ along the reference ellipsoid. The expression $\tan\emptyset$ accounts for latitude-dependent projection effects. The higher-order correction terms γA^4 and δA^6 are incorporated to further enhance projection accuracy, particularly for locations farther from the central meridian [17], [18].

After the conversion of GPS coordinates to the UTM system is complete, the position data is then converted to the local coordinate system in equations 3 and 4.

$$x = X - X_0 \quad (3)$$
$$y = Y - Y_0 \quad (4)$$

The initial position of the drone is used as the reference point (origin) with a value of (0,0) [19]. The variables x and y represent the drone's local coordinates relative to that starting point. Meanwhile, X and Y are the drone's UTM coordinates at a given time, while X_0 and Y_0 are the drone's initial UTM coordinates set as the origin (0,0). Thus, all subsequent drone positions are calculated relative to this starting point [20].

Next, the distance between the drone and the waypoint is calculated based on the local coordinate data (x, y) that has been obtained, as shown in Equation 5.

$$d = \sqrt{(X_w - x)^2 + (Y_w - y)^2} \quad (5)$$

The distance d is calculated based on the difference between the drone's local coordinates (x, y) and the waypoint coordinates (X_w, Y_w), as shown in the equation above. This distance value is used as a reference in the navigation system to determine how far the drone is from its target destination [21].

After obtaining the local coordinates (x, y) and the distance to the waypoint, the next step is to calculate the bearing angle using equations 6 and 7. This final step produces a compass bearing value that indicates the direction of the drone's movement toward the waypoint [22].

$$\theta = atan2(y_w - y,\ x_w - x) \quad (6)$$

$$bearing = \begin{cases} \theta . \frac{180}{\pi}, & \theta \geq 0 \\ \theta . \frac{180}{\pi} + 360, & \theta < 0 \end{cases} \quad (7)$$

Angle θ is calculated using the $atan2$ function based on the difference between the coordinates of the drone's position and the waypoint, as shown in equation (6). This function produces angles in radians within the range $-\pi$ to π. Next, the value of Θ is converted into degrees and normalized to a range of 0° to 360° using equation (7). The final result is a compass bearing value that indicates the direction of the drone's movement towards the waypoint.

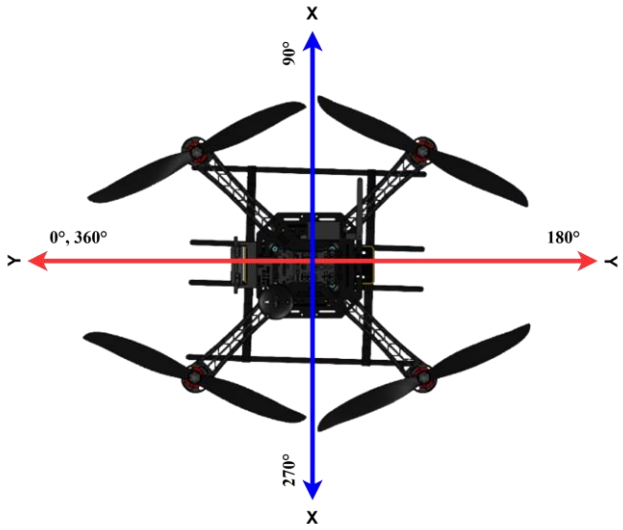

Figure 4. VTOL Yaw Orientation

The IMU-derived orientation value (yaw) represents the vehicle's heading relative to the reference axis, as illustrated in Figure 4. This yaw measurement is used in the bearing calculation to determine the UAV's directional alignment toward each waypoint. Prior to experimentation, the magnetometer was calibrated using the standard Pixhawk six-orientation calibration procedure to minimize hard-iron and soft-iron distortions. Accelerometer and gyroscope calibrations were also performed in accordance with the manufacturer's recommended procedures.

Since heading data were recorded under stabilized hovering conditions, long-term gyroscope drift accumulation was negligible. No additional external filtering algorithm was implemented beyond the default firmware-based filtering embedded within the flight controller.

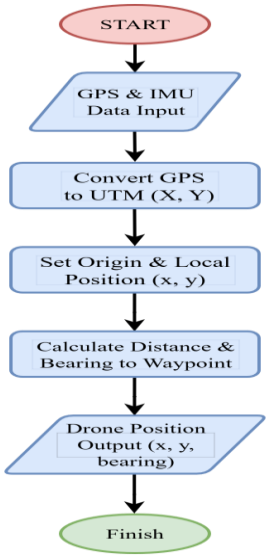

Figure 5. Flowchart of VTOL Localization System

Figure 5 shows the flowchart of the localization system on VTOL. The process begins with reading GPS and IMU data as system input. The GPS coordinate data is then converted into the UTM coordinate system (X,Y) [23]. Next, the initial position of the vehicle is set as the origin point, so that the global coordinates can be converted into local coordinates (X, Y) [24]. Based on these local coordinates, the system calculates the distance and bearing to the waypoint. The final result of this process is information on the position of the drone in local coordinates and the bearing value used as a reference for the direction of movement towards the target.

Based on these local coordinates, the system calculates the distance and bearing to the waypoint. The final result of this process is information about the drone's position in local coordinates and the bearing value used as a reference for the drone's movement towards the target [25].

D. Evaluation

Ground-truth reference distances were measured manually using a calibrated measuring tape between predefined waypoint markers on the ground. Each waypoint position was physically marked prior to flight testing to ensure consistent baseline measurement. The manual measurement accuracy is estimated to be within ±1 cm, which is sufficiently smaller than the GNSS standalone positioning uncertainty.

To evaluate the performance of the proposed localization system, two statistical metrics are employed: Root Mean Square Error (RMSE) and Sample Standard Deviation (SD). These complementary metrics provide a quantitative assessment of estimation accuracy and measurement consistency, respectively:

1) Root Mean Square Error (RMSE): RMSE quantifies the deviation between the estimated distance and the corresponding reference distance. It is widely adopted in localization performance analysis as a standard measure of estimation accuracy [26]. The RMSE for distance estimation is computed according to equation 8.

$$RMSE_{pos} = \sqrt{\frac{1}{N}\sum_{i=1}^{N}\left[\left(d_i - d_{ref}\right)^2\right]} \quad (8)$$

where N represents the total number of waypoint samples (N = 5) per testing scenario, d_i denotes the estimated distance at the i-th waypoint, $d_{ref,i}$ denotes the corresponding manually measured reference distance, and $e_i = d_i - d_{ref,i}$ represents the individual measurement error. RMSE provides an aggregated measure of the magnitude of estimation error by emphasizing larger deviations through quadratic weighting. A smaller RMSE value indicates better agreement between the estimated and reference distances.

It should be clarified that the reported RMSE values (0.017–0.047 m) do not represent absolute GPS positioning accuracy. Instead, they indicate the deviation between computed local distances derived from UTM-transformed coordinates and manually measured short-range reference distances within a predefined waypoint sequence. The GPS module operated in standalone mode under open-sky conditions without RTK or differential correction No additional external correction (RTK or DGPS) or custom filtering algorithm was applied beyond the default internal filtering implemented by the Pixhawk flight controller firmware. GPS position data were sampled at approximately 5 Hz and recorded once the UAV reached a stable hovering condition at each waypoint. Each recorded value corresponds to a stabilized position reading rather than a continuous trajectory average. Therefore, the evaluation reflects discrete short-range waypoint consistency under stabilized conditions. For each testing scenario, RMSE was calculated using five waypoint measurements (N = 5), corresponding to OH, WP1, WP2, WP3, and LD positions in accordance with competition mission rules. The experiment was repeated three times to evaluate consistency across trials. Distance values were recorded once the UAV reached a stable hovering condition at each waypoint. Therefore, the reported RMSE reflects short-range relative distance computation consistency rather than centimeter-level global positioning precision.

Therefore, the reported centimeter-level RMSE reflects short-range relative geometric consistency rather than absolute satellite-based positioning precision.

2) Sample Standard Deviation (SD): In addition to RMSE, the sample standard deviation (SD) is computed to evaluate the dispersion of individual error values across waypoint measurements. The mean error for distance estimation is first determined using Equations 9 and 10, which subsequently serves as the basis for calculating the sample standard deviation.

$$\bar{e} = \frac{1}{N} \sum_{i=1}^{N} e_i \quad (9)$$

The sample standard deviation is then calculated as:

$$SD = \sqrt{\frac{1}{N-1} \sum_{i=1}^{N} (e_i - \bar{e})^2} \quad (10)$$

where e_i represents the individual error at the i-th waypoint, and $\bar{e}$ denotes the mean error across all waypoint samples. The use of $N - 1$ in the denominator follows the sample standard deviation formulation, which is appropriate given the limited number of waypoint measurements per scenario. While RMSE provides the overall magnitude of estimation error, SD reflects the variability and consistency of localization performance across predefined mission targets.

Given the limited sample size (N = 5) per scenario, the statistical evaluation primarily reflects short-range experimental consistency rather than large-scale probabilistic inference. Therefore, the reported RMSE and SD values should be interpreted as indicators of local measurement stability under controlled open-sky conditions.

In addition to RMSE, the standard deviation (SD) is reported to describe the dispersion and repeatability of the observed errors. Given the limited sample size (N = 5 per test scenario), inferential statistical significance testing and confidence interval estimation were not performed. Therefore, the reported results should be interpreted as descriptive statistical indicators of short-range localization consistency under controlled experimental conditions rather than as inferential population-level conclusions.

III. Result and Discussion

This section presents and analyzes the experimental results obtained to evaluate the performance of the proposed localization system. The analysis focuses on three primary components: UTM coordinate transformation accuracy, distance estimation derived from GNSS-based positional data, and heading estimation obtained from the IMU sensor. These components are evaluated to assess the accuracy, consistency, and overall reliability of the localization system in supporting short-range waypoint navigation.

The GNSS receiver operated in standalone mode with a nominal horizontal accuracy of approximately 1.5–2.0 meters under open-sky conditions. Although standalone GNSS typically exhibits meter-level absolute positioning uncertainty, the evaluation in this study emphasizes short-range relative waypoint consistency within a limited operational radius rather than absolute global positioning accuracy.

A. UTM Data (X,Y) Experiment

The UTM (X, Y) data experiment was conducted to evaluate the stability and consistency of the local Cartesian coordinate representation derived from GPS latitude–longitude measurements. These transformed coordinates form the basis for distance and bearing calculations relative to the reference origin, constituting the core of the proposed UTM-based GPS–IMU localization framework. Any instability in the coordinate transformation may directly affect waypoint tracking accuracy and overall navigation performance.

The experimental results demonstrate generally consistent positional representation across repeated trials. However, minor variations are observed, particularly at WP2 and WP3 during Testing 3. These deviations may be attributed to inherent GNSS measurement noise or slight hovering instability during waypoint stabilization. Since the UTM transformation directly depends on GPS latitude–longitude inputs, fluctuations in satellite geometry or residual signal noise propagate into the local Cartesian coordinates. Nevertheless, the small magnitude of these variations indicates that the UTM-based transformation remains numerically stable for short-range waypoint navigation.

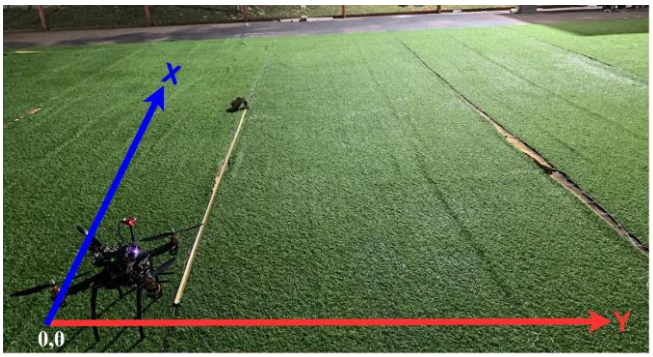

Figure 6. Experiment on Collecting X,Y and Distance Data

Figure 6 illustrates the experimental setup used to obtain the UAV position along the X and Y axes during the movement test. The UAV was initially placed at the origin (0, 0), which served as the reference point of the local coordinate system. The recorded X and Y positional data, defined according to the established coordinate convention, enable visualization of the UAV trajectory in the corresponding plot.

Table 1 presents the UTM coordinate data (X, Y) obtained from the GPS sensor at each target waypoint during the testing process. These values represent the UAV position in a local Cartesian coordinate system expressed in meters. The coordinate convention follows the defined navigation frame: lateral movement to the left corresponds to negative X values, forward movement corresponds to positive Y values, and backward movement corresponds to negative Y values.

TABEL I
EXPERIMENT DATA X,Y

Testing	Data X,Y					
	Testing 1		Testing 2		Testing 3	
	X(m)	Y(m)	X(m)	Y(m)	X(m)	Y(m)
OH	0.0	0.0	0.0	0.0	0.0	0.0
WP 1	-2.96	0.48	-2.96	0.48	-2.98	0.28
WP 2	-0.08	5.01	-0.08	5.01	-0.27	4.99
WP 3	1.5	-0.01	1.5	-0.01	1.54	-0.00
LD	0.45	-2.49	0.13	-2.42	0.45	-2.49

Although the UTM coordinates demonstrate generally consistent positioning across trials, minor variations are observed, particularly at WP1 and WP2. These deviations maybe attributed to inherent GNSS measurement jitter caused by satellite geometry variations and atmospheric effects. In addition, minor structural vibration during hovering and flight-controller stabilization adjustments may introduce short-term coordinate fluctuations. Since the system operates in standalone GNSS mode without differential correction, small positional noise directly propagates into the UTM-transformed local coordinates.

B. Data Distance Experiment

Distance testing was conducted to evaluate the accuracy of the computed distance between the UAV position and predefined waypoints using local coordinates generated by the localization system. The reference distance was measured manually using a measuring tape and compared with the distance calculated from UTM-based coordinates. The results of the distance evaluation are presented in Figure 6.

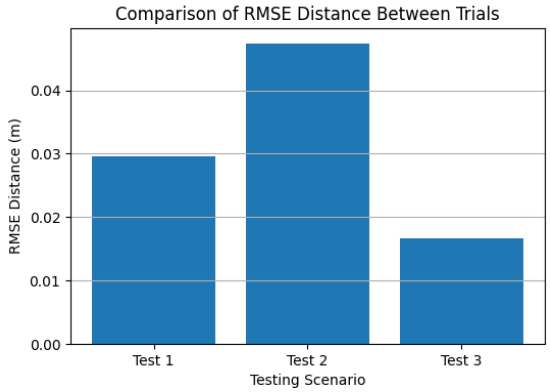

Figure 7. RMSE Distance Comparison Across Testing Scenario

Distance testing was conducted to evaluate the accuracy of the computed distance between the UAV position and predefined waypoints using local UTM-based coordinates generated by the localization system. The reference distance was measured manually using a measuring tape and compared with the distance calculated by the system. The results of the distance evaluation are presented in Figure 7.

It should be emphasized that the reported centimeter-level RMSE values represent relative short-range distance consistency over a limited 1–5 m baseline rather than absolute global GNSS positioning accuracy. The evaluation compares locally transformed UTM distances with manually measured short-range references under open-sky conditions. Therefore, the resulting RMSE primarily reflects the internal geometric consistency of the coordinate transformation and relative positioning rather than large-scale geodetic precision. The GNSS module operated in standalone mode without Real-Time Kinematic (RTK) correction or Differential GPS (DGPS) enhancement. No additional external correction methods were applied beyond the default internal filtering implemented within the Pixhawk flight controller firmware.

TABEL II
EXPERIMENT DISTANCE DATA

Testing	Jarak (M)			Aktual (M)	Error (M)		
	Tes 1	Tes 2	Tes 3		Tes 1	Tes 2	Tes 3
OH	0.0	0.0	0.0	0.0	0.0	0.0	0.0
WP 1	3.00	3.00	2.99	3.00	0.0	0.0	0.01
WP 2	5.01	5.01	4.99	5.00	0.01	0.01	0.01
WP 3	1.55	1.55	1.5	1.5	0.05	0.05	0.00
LD	2.53	2.42	2.53	2.5	0.05	0.08	0.03
RMSE					**0.030**	**0.047**	**0.017**
SD					**0.022**	**0.035**	**0.012**

C. Directional Data Experiment.

Testing the IMU Heading on Pixhawk against the compass heading is done to determine the heading (Yaw) value on the drone. The bearing data obtained from this test will then be integrated with position data to support the waypoint navigation process.

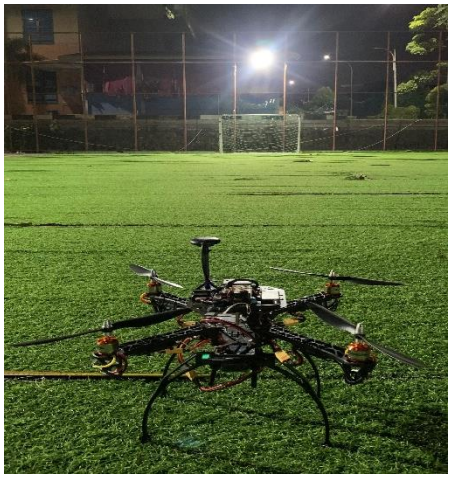

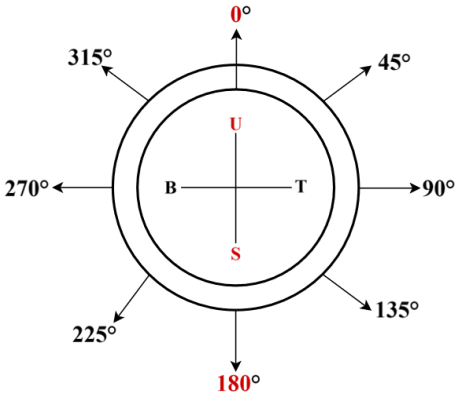

Figure 8. Heading Data Experiment

Figure 8 illustrates the heading data experiment conducted to evaluate the accuracy of yaw measurements obtained from the IMU sensor. During testing, the UAV was placed in an open-sky environment and oriented toward predefined compass reference angles. At each orientation, the corresponding yaw value reported by the IMU was recorded and compared with the reference direction. The angular difference between the measured and reference values was defined as the heading error and analyzed using the Root Mean Square Error (RMSE) method to quantify directional accuracy.

Prior to experimentation, the IMU magnetometer was calibrated using the standard Pixhawk calibration procedure to minimize magnetic bias. All measurements were collected while the UAV remained stationary on the ground to eliminate dynamic motion effects. Each recorded value therefore represents a stabilized yaw reading rather than a continuous dynamic measurement. Consequently, the reported RMSE values reflect static directional consistency under controlled open-sky conditions.

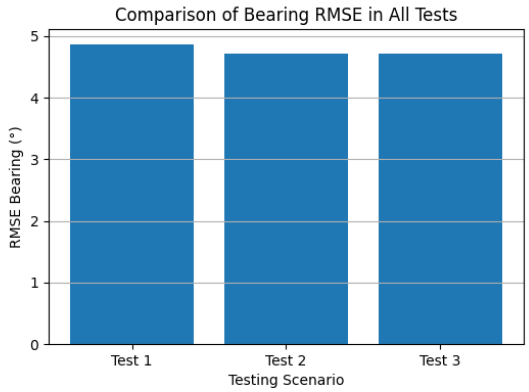

Figure 9. Bar Chart of RMSE Bearing for Each Testing Scenario

Figure 9 presents the Root Mean Square Error (RMSE) of the bearing angle for each test scenario. The RMSE was calculated from the difference between the yaw angle measured by the IMU and the corresponding reference direction. The largest deviation occurs at WP1, where a consistent 9° offset is observed across all trials, suggesting the presence of a systematic magnetic bias rather than random noise. In contrast, the smaller deviations at WP2 and WP3 indicate relatively stable directional estimation once the UAV is aligned closer to the intended heading.

Across the three experimental trials, the bearing RMSE remains within a narrow range of approximately 4–5°, while the low standard deviation (3.78°–3.83°) confirms good repeatability under static open-sky conditions. These findings demonstrate that the IMU-based heading estimation is sufficiently stable to support short-range waypoint navigation.

TABEL III
EXPERIMENT DISTANCE DATA

Testing	Bearing Data (°)						
	Tes 1	Tes 2	Tes 3	Aktual (°)	Error (°)		
OH	0°	0°	0°	0°	0°	0°	0°
WP 1	279°	279°	279°	270°	9°	9°	9°
WP 2	2°	2°	2°	0°	2°	2°	2°
WP 3	93°	92°	92°	90°	3°	2°	2°
LD	181°	180°	180°	180°	0°	0°	0°
RMSE					**4.87°**	**4.72°**	**4.72°**
SD					**3.83°**	**3.78°**	**3.78°**

All recorded bearing RMSE values remain within the predefined 5° benchmark established in the Introduction, thereby supporting the formulated hypothesis regarding directional consistency. A deeper analysis indicates that the observed deviations arise from practical physical and sensor-related factors. For distance estimation, residual GNSS measurement noise and satellite geometry variations (Dilution of Precision effects) may introduce short-term positional fluctuations, even under open-sky conditions. Minor hovering instability during waypoint stabilization may further contribute to small positional offsets.

For directional estimation, the systematic deviation observed at WP1 suggests residual magnetometer bias or local magnetic field distortion. Despite prior calibration, magnetic interference from onboard electronics or nearby metallic structures may affect yaw measurements. In addition, small synchronization delays between GNSS position updates and IMU heading data may introduce minor temporal inconsistencies during data logging. Collectively, these factors explain the small but consistent deviations observed in both distance and bearing RMSE results, indicating that the measured errors originate from inherent sensor limitations rather than instability in the proposed UTM-based localization framework. Overall, the system demonstrates stable short-range waypoint consistency under controlled open-sky conditions within the defined operational scope.

It should be noted that the evaluation was limited to discrete waypoint hovering rather than continuous trajectory tracking. Dynamic flight behaviors such as acceleration, deceleration, and rapid heading changes were not explicitly analyzed. Moreover, the system was not tested under GNSS-

degraded conditions, including partial satellite obstruction, multipath-rich urban environments, or intentional signal interference. Therefore, the findings should be interpreted within the context of short-range open-field VTOL operations. Future work will focus on continuous trajectory evaluation, dynamic error modeling, and robustness testing under degraded signal conditions to further validate the proposed localization framework.

D. Limitations and Future Work

The developed localization system demonstrates effective operation in open-sky environments with minimal signal interference, indicating reliable performance under controlled conditions. Nevertheless, several limitations must be acknowledged. The experimental evaluation was conducted exclusively in open-field environments and did not consider more challenging scenarios such as enclosed spaces, dense vegetation, tunnels, or urban areas with high building density. The system was primarily designed and optimized for open-area applications, as typically encountered in KRTI competition settings. Consequently, its performance under signal obstruction, multipath propagation, or electromagnetic interference has not been systematically evaluated.

In addition, validation was limited to discrete waypoint hovering conditions rather than continuous trajectory tracking. System performance was assessed only at predefined mission points (OH, WP1, WP2, WP3, and LD), without analyzing cumulative positioning error during sustained flight. Dynamic flight factors—including velocity-induced deviation, wind disturbances, and potential time-synchronization delays between GPS and IMU measurements—were not explicitly investigated. Therefore, the reported results primarily reflect short-range static waypoint accuracy under controlled open-sky conditions, rather than long-term navigation robustness in complex operational environments.

IV. CONCLUSION

This study has successfully developed and experimentally evaluated a deterministic UTM-based GPS–IMU localization framework for short-range waypoint navigation of a VTOL UAV. By transforming GPS latitude–longitude measurements into a local Cartesian coordinate system and integrating IMU-derived yaw information for heading estimation, the proposed system enables efficient computation of relative distance and bearing toward predefined waypoints.Experimental results obtained under controlled open-sky conditions demonstrate distance RMSE values ranging from 0.017 m to 0.047 m and bearing RMSE within 4–5°, satisfying the predefined performance benchmark of distance RMSE below 0.1 m and bearing RMSE within 5°. It is important to emphasize that these centimeter-level RMSE values represent short-range relative geometric consistency derived from UTM-transformed local coordinates, rather than absolute GNSS positioning accuracy, as the system operates in standalone mode without RTK or differential correction.The findings indicate that, for open-field VTOL missions with limited operational radius, deterministic coordinate transformation combined with GPS–IMU heading estimation can provide sufficient navigation stability without implementing additional probabilistic sensor-fusion algorithms. This highlights the practical viability of a lightweight and computationally simple localization approach for competition-based and open-area UAV applications.

However, the current evaluation is limited to discrete hovering conditions and open-sky environments. Continuous trajectory tracking, dynamic flight conditions, and GNSS-degraded scenarios were not investigated. Future work will focus on dynamic performance evaluation and robustness testing under challenging operational environments to further assess and extend the applicability of the proposed framework.

REFERENCES

[1] M. Idrissi, M. Salami, and F. Annaz, "A review of quadrotor unmanned aerial vehicles: Applications, architectural design and control algorithms," J. Intell. Robot Syst., vol. 104, Art. no. 22, 2022, doi: 10.1007/s10846-021-01527-7.

[2] A. C. Subrata, "Automatic landing and waypoint system berbasis kombinasi GPS dan mesin visi untuk multirotor pada Kontes Robot Terbang Indonesia divisi vertical take off landing," J. Ilm. Tek. Elektro Komput. dan Inform. (JITEKI), vol. 2, no. 2, pp. 110–122, Dec. 2016, doi: 10.26555/jiteki.v2i2.4896.

[3] C. Chi, X. Zhan, S. Wang, and Y. Zhai, "Enabling robust and accurate navigation for UAVs using real-time GNSS precise point positioning and IMU integration," Aeronaut. J., vol. 124, no. 1278, pp. 1–22, 2020, doi: 10.1017/aer.2020.80.

[4] Y. S. Wang, X. Zhang, and L. Chen, "UAV sensor data fusion for localization using adaptive multiscale feature matching mechanisms," Aerospace, vol. 12, no. 12, pp. 1–18, 2025, doi: 10.3390/aerospace12121048.

[5] Y. Chang, Y. Cheng, U. Manzoor, and J. Murray, "A review of UAV autonomous navigation in GPS-denied environments," Robot. Auton. Syst., vol. 170, Art. no. 104533, 2023, doi: 10.1016/j.robot.2023.104533.

[6] H. Zhang, L. Wang, and J. Li, "Review of AI-based UAV navigation in GPS-denied environments," in Proc. Int. Conf. Artif. Intell., 2024, pp. 1–8.

[7] W. Jang, M. Cho, H. Lim, and S. Lee, "Vision-based optimal landing guidance law for VTOL UAVs on a moving platform," Int. J. Aeronaut. Space Sci., vol. 26, pp. 1708–1731, 2025, doi: 10.1007/s42405-024-00825-2.

[8] R. Mahony, V. Kumar, and P. Corke, "Multirotor aerial vehicles: Modeling, estimation, and control," IEEE Robot. Autom. Mag., vol. 23, no. 2, pp. 20–32, 2016.

[9] S. Bouabdallah, P. Murrieri, and R. Siegwart, "Design and control of quadrotors with application to autonomous flying," Annu. Rev. Control, vol. 44, pp. 20–32, 2017, doi: 10.1016/j.arcontrol.2017.09.004.

[10] G. Hoffmann et al., "Quadrotor helicopter flight dynamics and control," in AIAA Guid., Navig., Control Conf., 2016.

[11] L. Meier et al., "PX4: A node-based multithreaded open source robotics framework," in Proc. IEEE Int. Conf. Robot. Autom. (ICRA), 2018, pp. 1–8.

[12] Y. Zhang et al., "GPS/INS integrated navigation systems: A review," J. Navig., vol. 70, no. 1, pp. 1–19, 2017, doi: 10.1017/S0373463316000412.

[13] R. Beard and T. McLain, "Guidance, navigation, and control of fixed-wing and multirotor UAVs," IEEE Control Syst. Mag., vol. 37, no. 2, pp. 33–46, 2017, doi: 10.1109/MCS.2017.2676316.
[14] Y. Sun et al., "Design and implementation of a UAV navigation system based on GPS/IMU integration," Sensors, vol. 18, no. 10, Art. no. 3416, 2018, doi: 10.3390/s18103416.
[15] M. Ryll, H. H. Bülthoff, and P. R. Giordano, "A novel overactuated quadrotor UAV: Modeling, control, and experimental evaluation," IEEE Trans. Control Syst. Technol., vol. 29, no. 6, pp. 2568–2581, 2021, doi: 10.1109/TCST.2020.3005857.
[16] C. F. F. Karney, "Algorithms for geodesics," J. Geodesy, vol. 89, no. 1, pp. 43–55, 2015, doi: 10.1007/s00190-014-0766-0.
[17] Z. Li, S. Bian, Q. Liu, H. Li, C. Chen, and Y. Hu, "Nonzonal expressions of Gauss–Krüger projection in polar regions," ISPRS Ann. Photogramm. Remote Sens. Spatial Inf. Sci., vol. III-4, pp. 11–15, 2016, doi: 10.5194/isprs-annals-III-4-11-2016.
[18] O. Lewicka et al., "Analysis of transformation methods of hydroacoustic and geospatial data," Remote Sens., vol. 14, no. 7, 2022, doi: 10.3390/rs14071618.
[19] A. Elamin, N. Abdelaziz, and A. El-Rabbany, "A GNSS/INS/LiDAR integration scheme for UAV-based navigation in GNSS-challenging environments," Sensors, vol. 22, no. 24, Art. no. 9908, 2022, doi: 10.3390/s22249908.
[20] A. Tonini, M. Castelli, J. S. Bates, N. N. N. Lin, and M. Painho, "Visual-inertial method for localizing aerial vehicles in GNSS-denied environments," Appl. Sci., vol. 14, no. 20, Art. no. 9493, 2024, doi: 10.3390/app14209493.
[21] M. de Berg, J. Snoeyink, and M. van Kreveld, "Waypoint navigation of mobile robots using distance and bearing control," arXiv preprint arXiv:1803.05447, 2018.
[22] J. Kim, S. Lee, and H. Kim, "Design of waypoint navigation and guidance system for UAV," Appl. Sci., vol. 10, no. 9, Art. no. 3070, 2020, doi: 10.3390/app10093070.
[23] M. P. Christiansen et al., "Designing and testing a UAV mapping system for accurate pose estimation," Sensors, vol. 17, no. 12, Art. no. 2703, 2017, doi: 10.3390/s17122703.
[24] Y. Yao et al., "UAV geo-localization dataset and method based on cross-view matching," Sensors, vol. 24, no. 21, Art. no. 6905, 2024, doi: 10.3390/s24216905.
[25] Y. Yang, "UAV waypoint opportunistic navigation in GNSS-denied environments," M.S. thesis, Ohio State Univ., Columbus, OH, USA, 2022.
[26] R. S. Wijaya, E. R. Jamzuri, A. Wibisana, J. A. Sinaga, and V. Julanba, "Sensor fusion–based localization for ASV with linear regression optimization," J. Appl. Inform. Comput., vol. 9, no. 4, pp. 1991–1999, 2023, doi: 10.30871/jaic.v9i4.10048.